Electronic Supplementary Information

# Enhancing Energy Storage Capacity of Graphene Supercapacitors via Solar Heating

Xinling Yu,‡[ac] Nian Li,‡[ac] Shudong Zhang,[ac] Cui Liu,[ac] Liqing Chen,[abc] Min Xi,[ac] Yanping Song,[abc] Sarmad Ali,[ac] Obaid Iqbal,[ac] Mingyong Han[d], Changlong Jiang[ac] and Zhenyang Wang*[ac]

[a]Institute of Solid-State Physics, Chinese Academy of Sciences, Hefei, Anhui 230031, China

[b]Department of Chemistry, University of Science and Technology of China, Hefei, Anhui 230026, China

[c]Key Laboratory of Photovoltaic and Energy Conservation Materials, Hefei Institutes of Physical Science, Chinese Academy of Sciences, Hefei 230031, China

[d]Institute of Molecular Plus, Tianjin University, Tianjin 300072, China

‡These authors contributed equally to this work.

* Corresponding author.
zywang@iim.ac.cn (Zhenyang Wang)

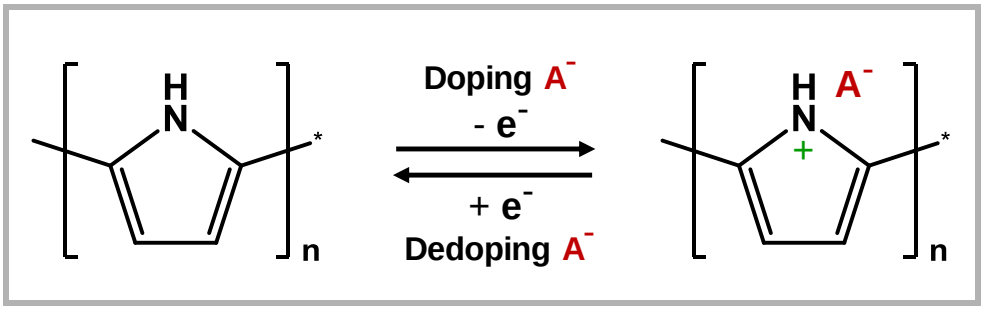


**Note S1** Faradaic reaction of the PPy in the ST-MSC

The conducting polymers polypyrrole (PPy) provides the pseudocapacitance from a Faradaic process on its surface through the doping/dedoping reaction, $A^-$ represents the negative ions such as $PTS^-$, $SO_4^{2-}$, and so on.

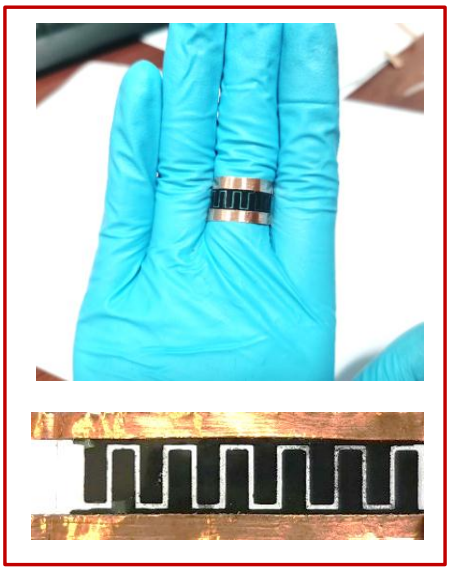

**Fig. S1** Photograph of the flexible ST-MSC worn on the finger.

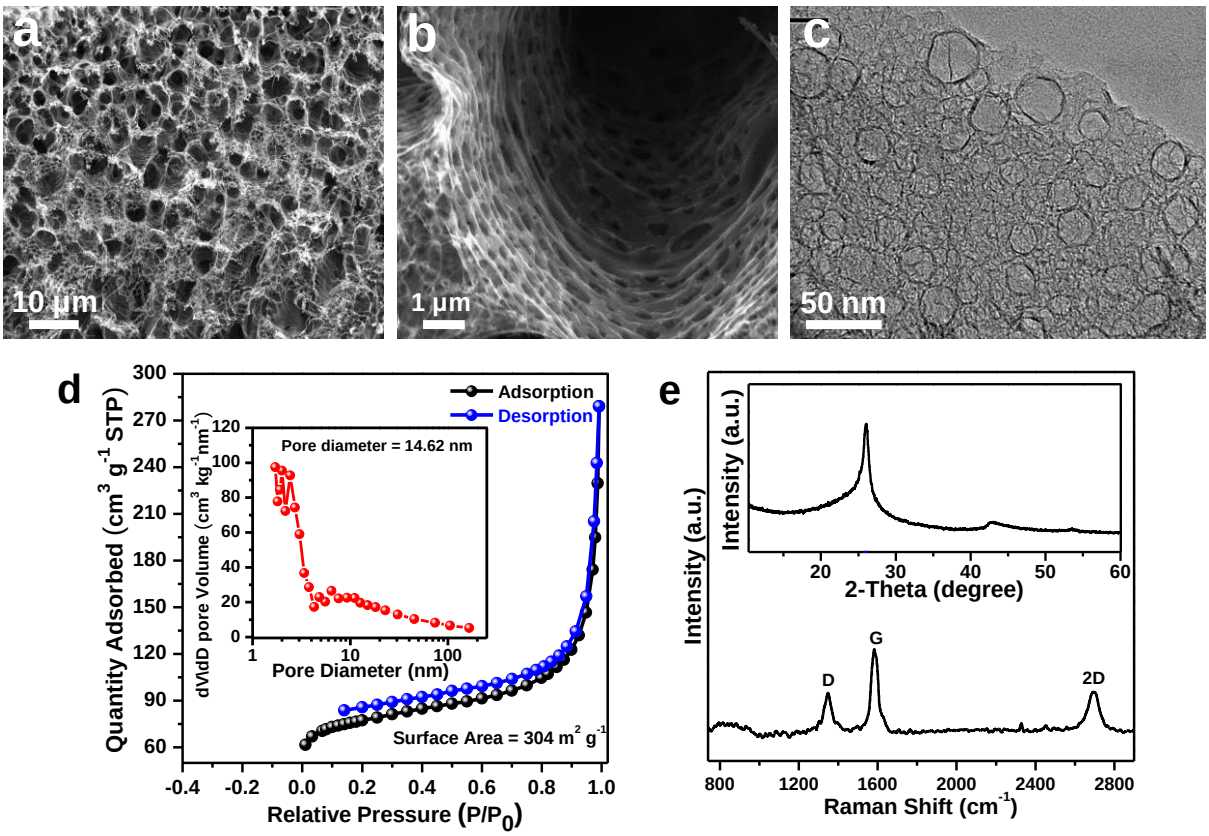


**Fig. S2** Morphology characterizations of the LIG. The SEM images (a, b) and TEM image (c). (d) $N_2$ adsorption/desorption isotherm and pore size distribution. (e) XRD and Raman spectroscopy.

The LIG can be characterized by the characteristic peaks at 1349 $cm^{-1}$ (D band, disorder and defective nature of graphene), 1583 $cm^{-1}$ (G band, graphitic $sp^2$ carbon) and 2706 $cm^{-1}$ (2D band, alteration of the electronic band structure resulted from the interactions between the graphene layers). The low $I_D/I_G$ of the LIG indicates the graphitic structure [1-3]. XRD analysis confirms the graphitization of LIG by two distinct peaks at 26 ° and 43.2 °, corresponding to the typical (002) and (100) lattice planes of crystallized graphite, respectively [4-6].

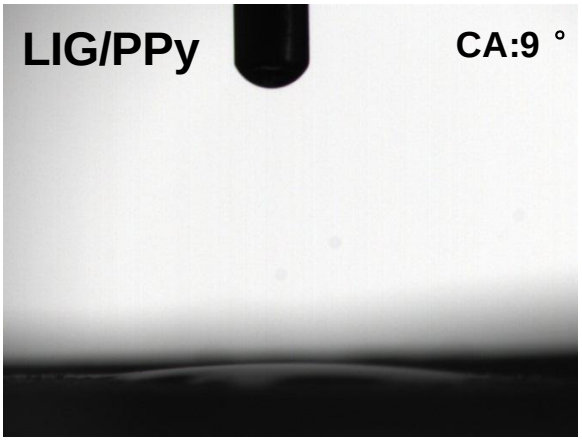


**Fig. S3** Contact angle of water on LIG/PPy-15000.

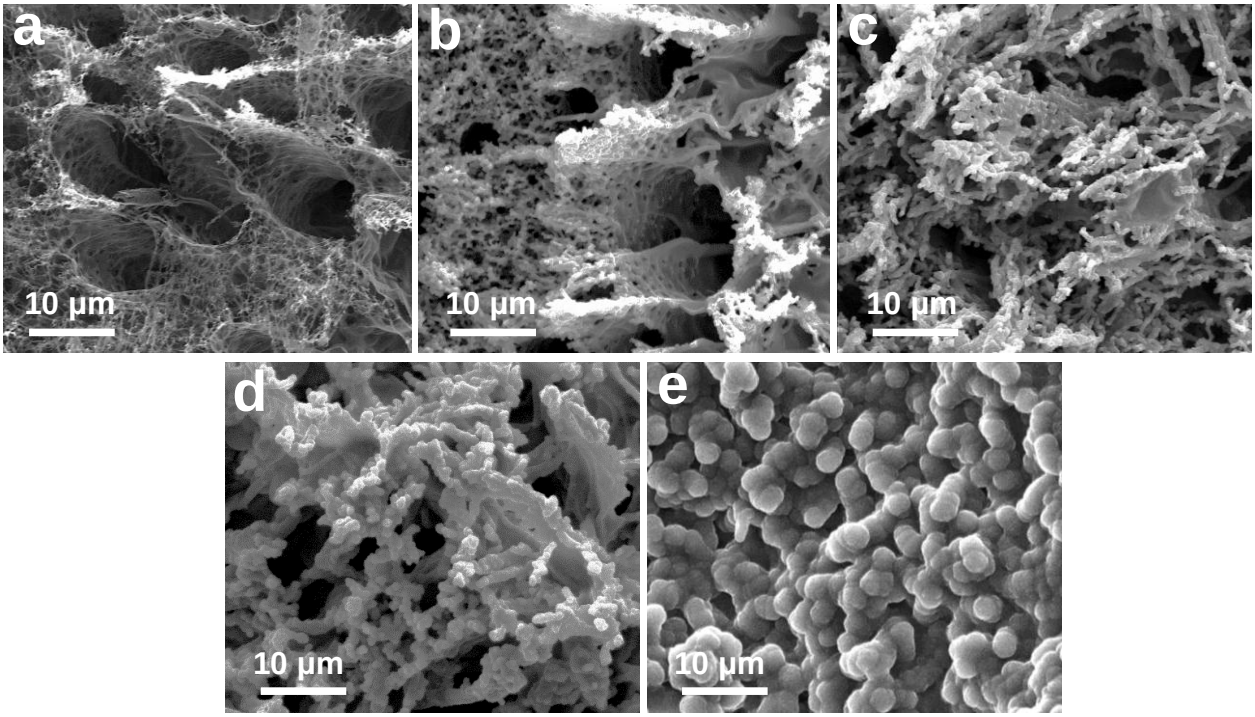


**Fig. S4** Top view of SEM images of (a) LIG, (b) LIG/PPy-5000, (c) LIG/PPy-10000, (d) LIG/PPy-15000, and (e) LIG/PPy-20000.

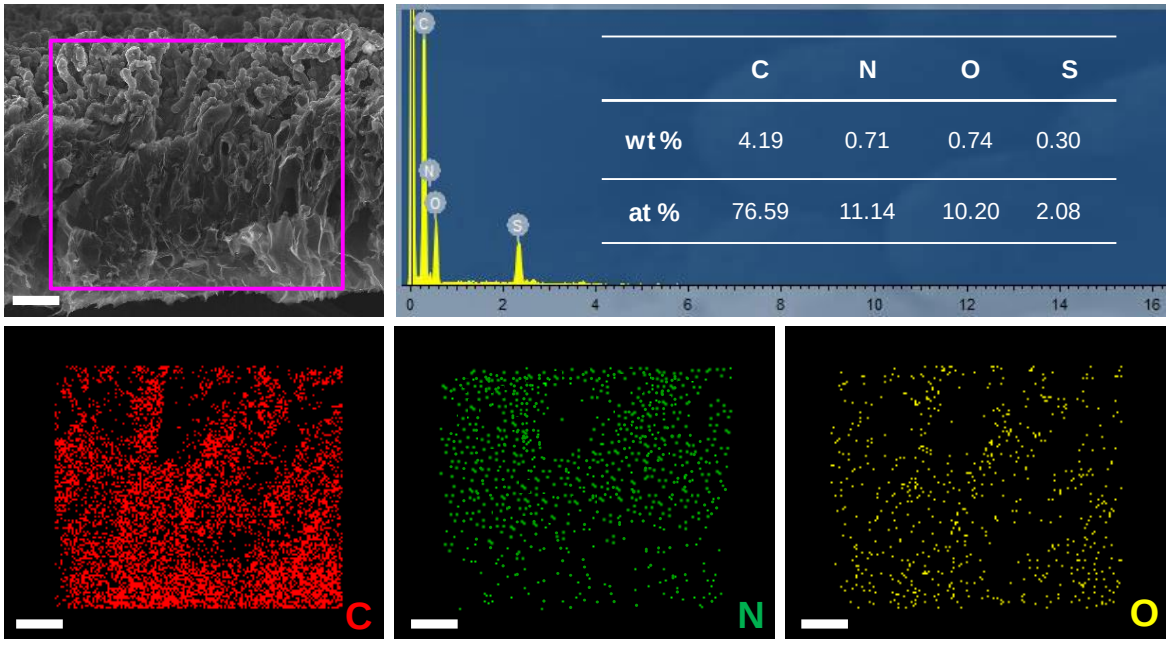


| | C | N | O | S |
|---|---|---|---|---|
| wt % | 4.19 | 0.71 | 0.74 | 0.30 |
| at % | 76.59 | 11.14 | 10.20 | 2.08 |

**Fig. S5** The cross-sectional SEM image and the corresponding EDS elemental mappings of LIG/PPy-15000 composite, the scale bars are 50 μm.

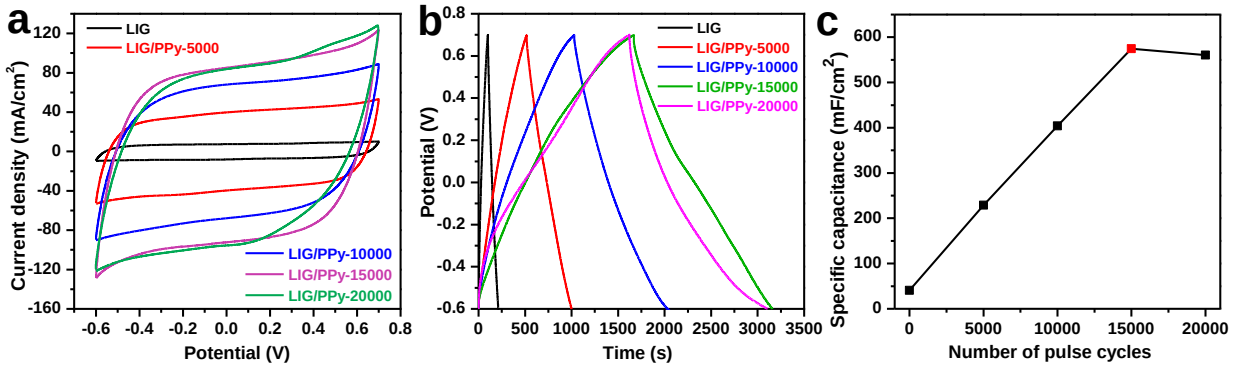


**Fig. S6** (a) CV curves of ST-MSC based on LIG/PPy-X electrode, the scan rate is 200 mV $s^{-1}$. (b) GCD curves of LIG and LIG/PPy-X, the current density is 0.5 mA $cm^{-2}$. (c) The areal specific capacitances of LIG and LIG/PPy-X calculated from the GCD curves at the current density is 0.5 mA $cm^{-2}$.

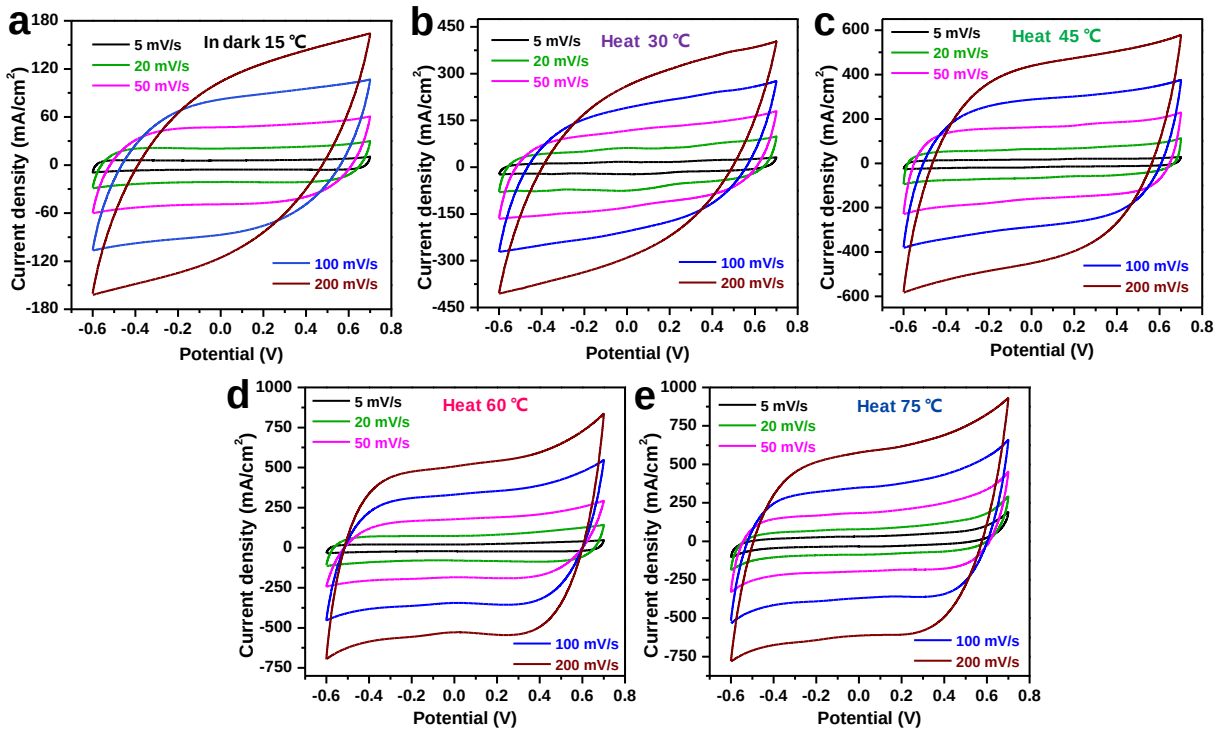


**Fig. S7** (a) CV curves of ST-MSC in dark (15 ℃). CV curves of ST-MSC at the heating temperature of (b) 30 ℃, (c) 45 ℃, (d) 60 ℃, and (e) 75 ℃ at the scan rate range of 5 and 200 mV/s.

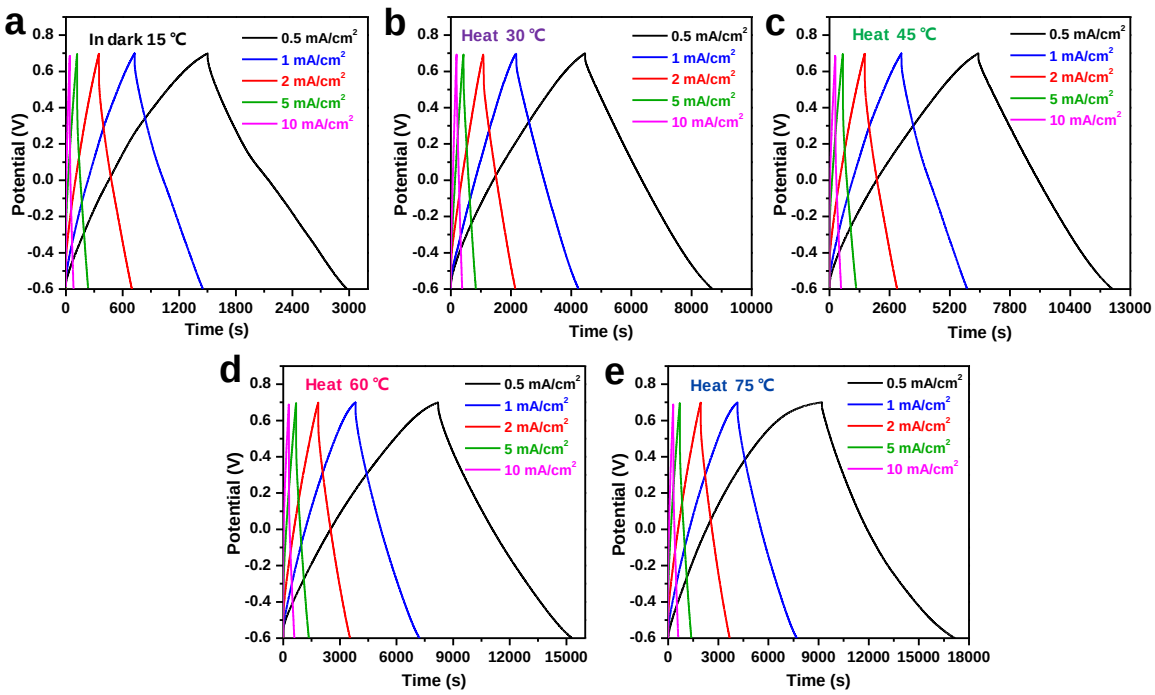


**Fig. S8** (a) GCD curves of ST-MSC in dark 15 ℃. GCD curves of ST-MSC at the heating temperature of (b) 30 ℃, (c) 45 ℃, (d) 60 ℃, and (e) 75 ℃ at the current density range of 0.5 and 10 mA/cm$^2$.

**Table S1** Comparison of capacitance, energy density, power density, and stability of reported MSC based on graphene composite electrodes

| **Electrode** | **Specific capacitance (mF/cm$^2$)/(F/cm$^3$)** | **Energy density (μWh/cm$^2$)/(mWh/cm$^3$)** | **Power density (μW/cm$^2$)/(mW/cm$^3$)** | **Capacitence retention** | **Ref.** |
|---|---|---|---|---|---|
| LIG/PANI | 90.3/11.88 at 0.5 mA/cm$^2$ | 8.0/1.05 | 629.5/82.83 | 97 % after 6000 cycles | [7] |
| LIG/$MnO_2$ | 233.4/23.35 at 0.5 mA/cm$^2$ | 32.4/3.21 | 2334.0/231.1 | 82 % after 6000 cycles | [7] |
| PPy/GF | 89.6/~0.48 at 0.6 mA/cm$^2$ | 24/~0.13 | 390/~2.09 | ~75 % after 10000 cycles | [8] |
| rGO/PPy | 9.4/-- at 0.17 mA/cm$^2$ | 20/-- | 40/-- | 87 % after 2000 cycles | [9] |
| rGO/PPy | 512/59.9 at 1.0 mA/cm$^2$ | 61.4/7.18 | 10/1.17 | 82.7 % after 10000 cycles | [10] |
| LIG/PPy | 574/19.1 (R.T., 15 ℃) 2755.2/91.84 (60 ℃) 2752.3/91.74 (R.T., under 1 solar irradiation) at 0.5 mA/cm$^2$ | 134.7/4.49 (R.T., 15 ℃) 646.6/21.56 (60 ℃) 646.0/21.53 (R.T., under 1 solar irradiation) | 6500/216.7 | 96.3 % (R.T., 15 ℃) 86.0 % (60 ℃) 85.8 % (R.T., under 1 solar irradiation) after 10000 cycles | This work |

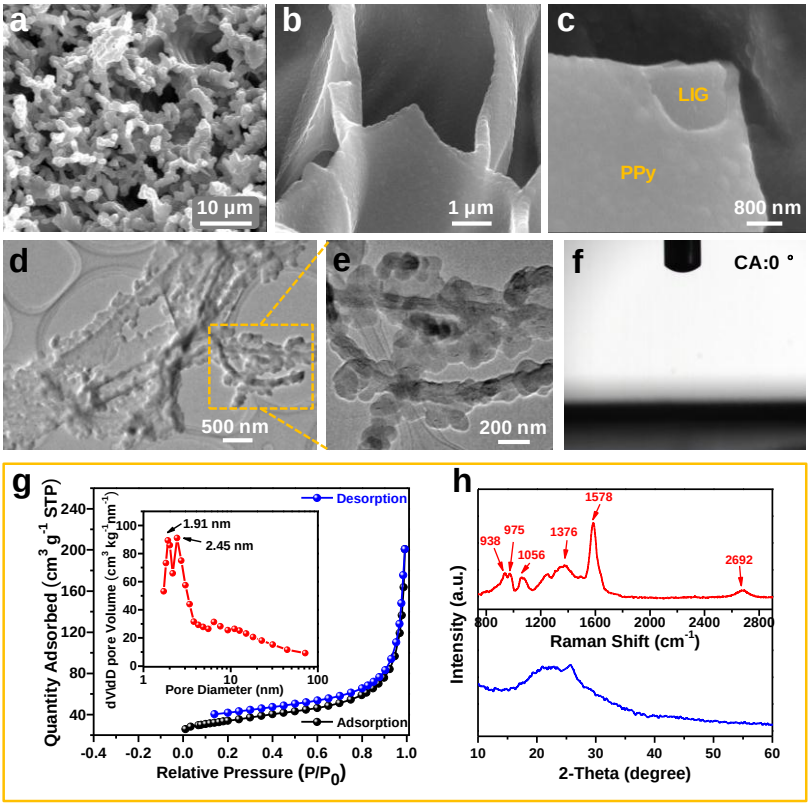


**Fig. S9** The structural and morphological characterizations of the LIG/PPy-15000 after 10000 GCD cycles at 60 ℃. (a-c) The SEM images of LIG/PPy-15000 at different magnifications. (d and e) The TEM images of LIG/PPy-15000 at different magnifications. (f) Contact angle of water on LIG/PPy-15000. (g) $N_2$ adsorption/desorption isotherm and pore size distribution of LIG/PPy-15000. (h) XRD and Raman patterns of LIG/PPy-15000.

No obvious changes were observed in the structures and morphologies of electrode material before and after the electrochemical studies at 60 ℃, indicating the good stability of the electrode material to temperature.

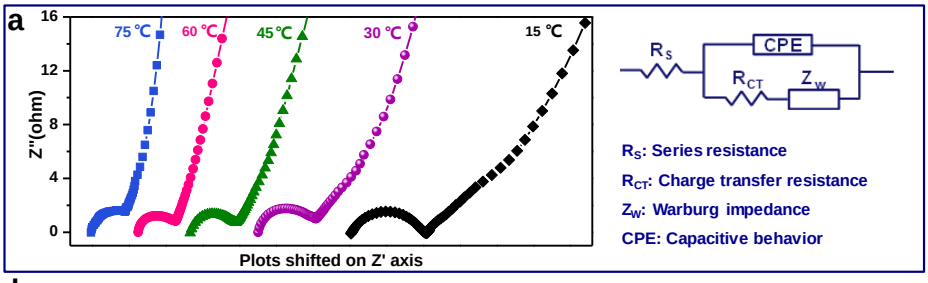


b

| Parameters | 15 ℃ | 30 ℃ | 45 ℃ | 60 ℃ | 75 ℃ |
|---|---|---|---|---|---|
| $R_S$/Ω | 7.21 | 6.43 | 5.62 | 4.92 | 4.24 |
| $R_{CT}$/Ω | 1.7 | 1.4 | 1.1 | 0.9 | 0.7 |

**Fig. S10** (a) Nyquist spectra of panel a showing the semicircles plotted on the shifted real axis for clarity (left); The equivalent circuit model (right). (b) Parameter results simulated by the equivalent circuit model.

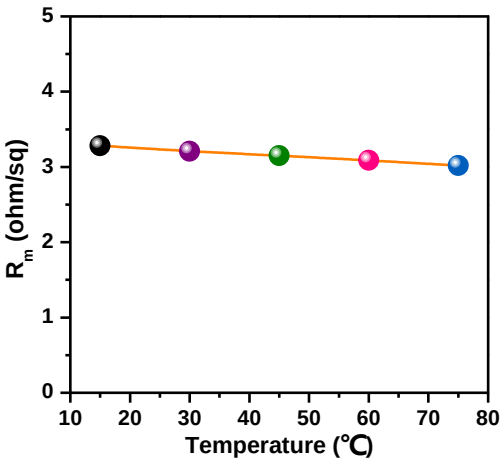


**Fig. S11** The change of the $R_m$ value when the temperature rises from 15 to 75 ℃.

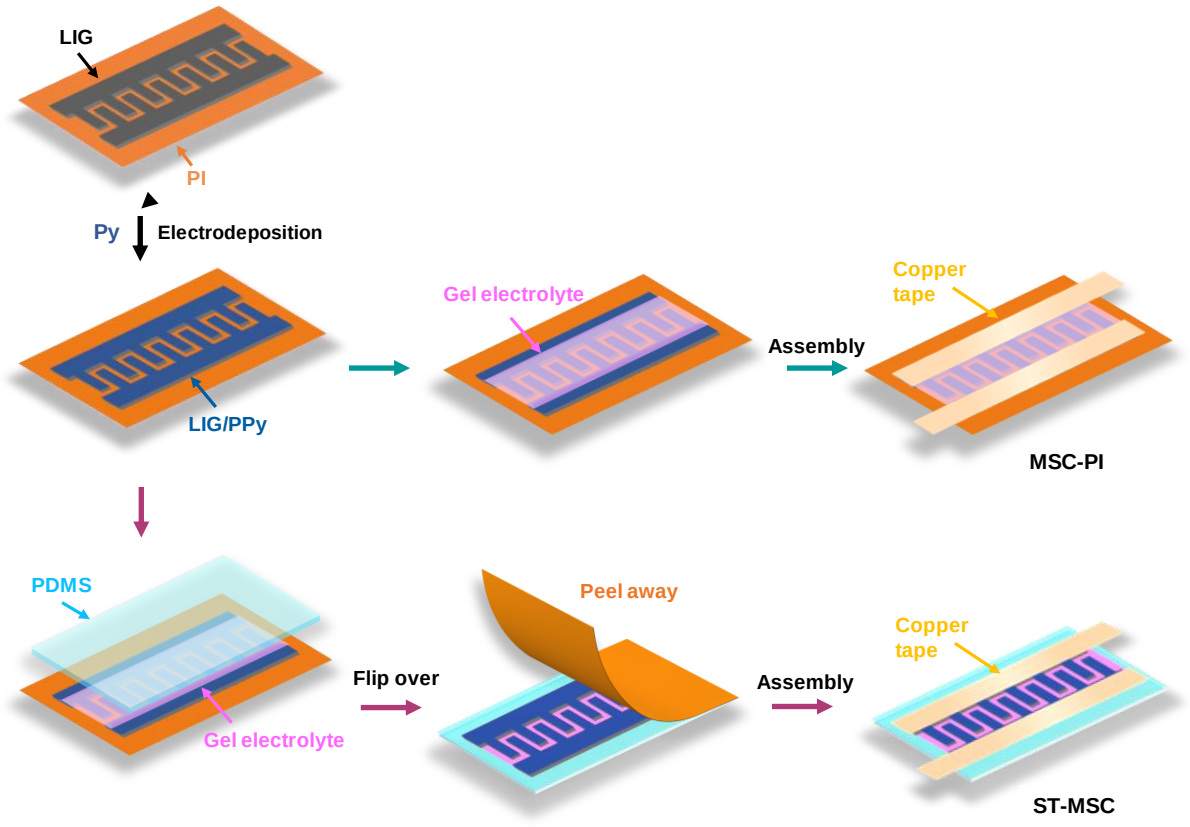


**Fig. S12** Fabrication of two different structures MSCs: MSC-PI and ST-MSC.

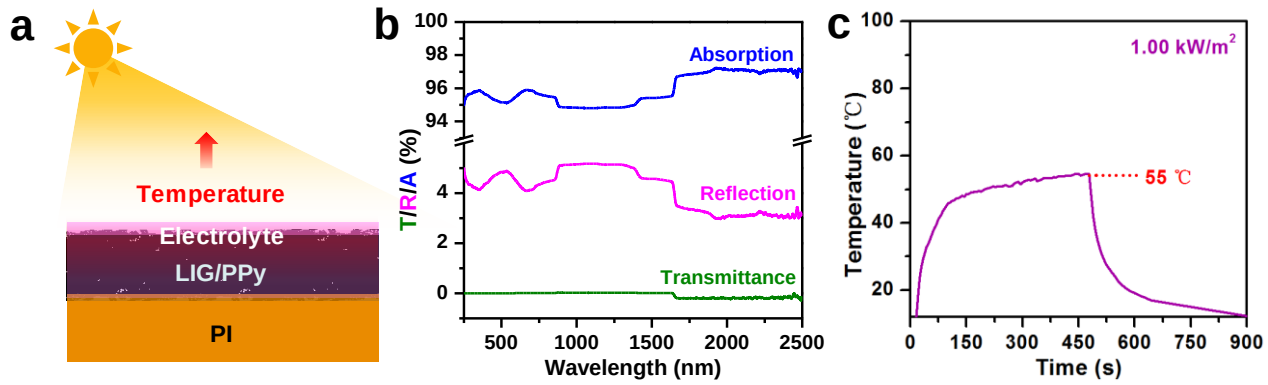


**Fig. S13** (a) Schematic cross-section of the MSC-PI. (b) UV-vis-NIR transmittance (T), reflectance (R), and absorption (A) spectra of the MSC-PI. (c) Time-courses of the MSC-PI under solar irradiation at a light intensity of 1.00 kW $m^{-2}$.

The solar-thermal conversion efficiency (η) is calculated according to the following equation:

$$\eta = [h\, S_{MSC}\, (T_{max}-T_0)- Q_S]/I(1-10^{-A}) \quad \text{(S1)}$$

$$\tau = \sum M_e\, C_e\, /h\, S_{MSC} \quad \text{(S2)}$$

where $h$ is the heat-transfer coefficient, $S_{MSC}$ is the area of the MSC, $T_{max}$ is the maximum temperature in steady state, $T_0$ is ambient temperature, $Q_S$ is the thermal energy dissipated to the surrounding per unit time, $I$ is the simulated solar light intensity, A is the absorbance of the MSC over the entire solar spectrum, $\tau$ is the system time constant, $M_e$ and $C_e$ are the mass and heat capacity of electrode material and electrolyte, respectively. The detailed calculation parameters of $\eta$ are listed in Table S1.

**Table S2** The detailed calculation parameters of $\eta$ of MSCs.

| **Parameter** | $T_0$ | $I$ | $C_{LIG}$ | $C_{PPy}$ | $C_{GE}$ |
|---|---|---|---|---|---|
| **MSCs** | 288.15 K | 1.00 kW/$m^2$ | 1.34 J/kg/K | 1.34 J/kg/K | 5 J/kg/K |
| **Parameter** | $T_{max}$ (K) | $A$ | $M_{LIG}$ | $M_{PPy}$ | $M_{GE}$ |
| **ST-MSC** | 348.2 | 98.8 % | 1.2 mg | 5.1 mg | 300 mg |
| **MSC-PI** | 338.5 | 95.9 % | 1.2 mg | 5.1 mg | 300 mg |

$M_{LIG}$, $M_{PPy}$, and $M_{GE}$ are the mass of LIG, PPy, and Gel Electrolyte of the MSC-PI and ST-MSC, respectively;

$C_{LIG}$, $C_{PPy}$, and $C_{GE}$ are the heat capacity of LIG, PPy, and Gel Electrolyte of the MSC-PI and ST-MSC, respectively.

**Table S3** The comparison of transmittance (T), reflectance (R), absorption (A), solar-thermal conversion efficiency (η), and the surface temperature change (ΔT, under the solar irradiation at a light intensity of 1.00 kW $m^{-2}$) of the MSC-PI and ST-MSC.

| | Transmittance (T) | Reflectance (R) | Absorption (A) | Solar-thermal conversion efficiency (η) | Temperature change (ΔT) |
|---|---|---|---|---|---|
| **ST-MSC** | 0.1 % | 0.1 % | 98.9 % | 23.5 % | 45 ºC |
| **MSC-PI** | 0.1 % | 4.3 % | 95.6 % | 22.8 % | 40 ºC |

## Electrochemical measurements

All electrochemical tests including cyclic voltammetry (CV), galvanostatic charge discharge (GCD), and electrochemical impedance spectroscopy (EIS) were performed on a CHI 660E electrochemical workstation (Shanghai CH Instrument Company, China). The areal specific capacitance ($C_{MSC,A}$) and volumetric specific capacitance ($C_{MSC,V}$) of the MSC were calculated from GCD curves according to equations S3 and S4, respectively:

$$C_{MSC,A} = I/(A_{MSC} \times (dV/dt) \quad (S3)$$

$$C_{MSC,V} = I/(V_{MSC} \times (dV/dt) \quad (S4)$$

where, I (mA) was the discharge current; dV/dt was the slope of galvanostatic discharge curves; $A_{MSC}$ ($cm^2$) and $V_{MSC}$ ($cm^3$) were the area and volume of the MSC, respectively.

The areal energy density ($E_{MSC,A}$) and volumetric energy density ($E_{MSC,V}$) of the MSC device were calculated by using equations S5 and S6, respectively:

$$E_{MSC,A} = C_{MSC,A}V^2/(2 \times 3600) \quad (S5)$$

$$E_{MSC,V} = C_{MSC,V}V^2/(2 \times 3600) \quad (S6)$$

where V was the potential difference of the full discharge process.

The areal power densities ($P_{MSC,A}$) and volumetric energy density ($P_{MSC,V}$) of the MSC device were calculated by using equations S7 and S8, respectively:

$$P_{MSC,A} = 3600\ E_{MSC,A}/t \quad (S7)$$

$$P_{MSC,V} = 3600\ E_{MSC,V}/t \quad (S8)$$

where *t* is the time spent in full discharge.

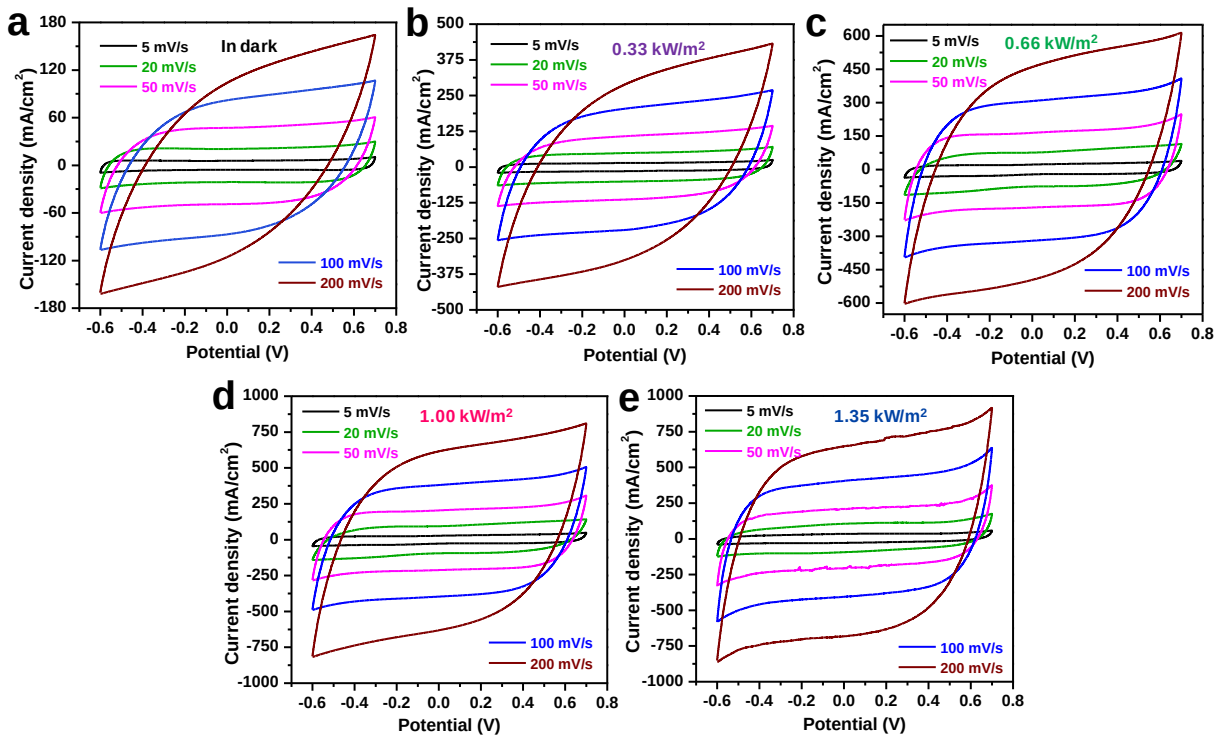


**Fig. S14** (a) CV curves of ST-MSC in dark. CV curves of MSC under (b) 0.33 kW/m$^2$, (c) 0.66 kW/m$^2$, (d) 1.00 kW/m$^2$, and (e) 1.35 kW/m$^2$ at the scan rate range of 5 and 200 mV/s.

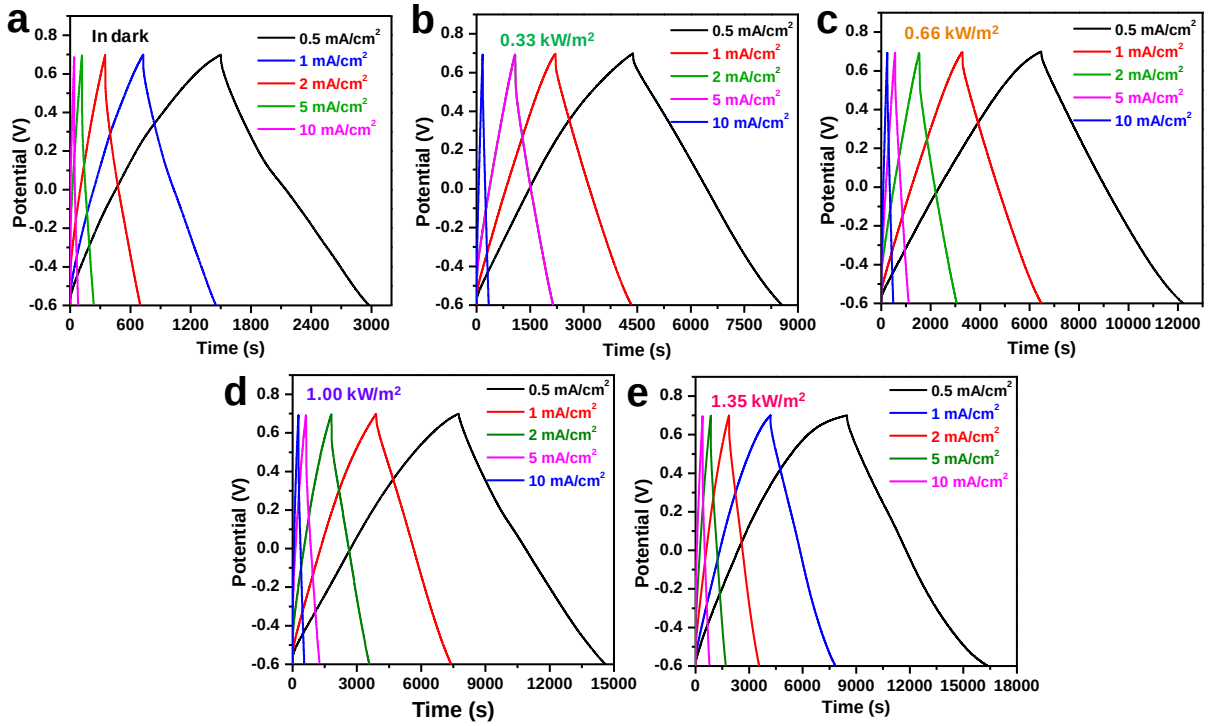


**Fig. S15** (a) GCD curves of ST-MSC in dark. GCD curves of MSC under (b) 0.33 kW/m$^2$, (c) 0.66 kW/m$^2$, (d) 1.00 kW/m$^2$, and (e) 1.35 kW/m$^2$ at the current density range of 0.5 and 10 mA/cm$^2$.

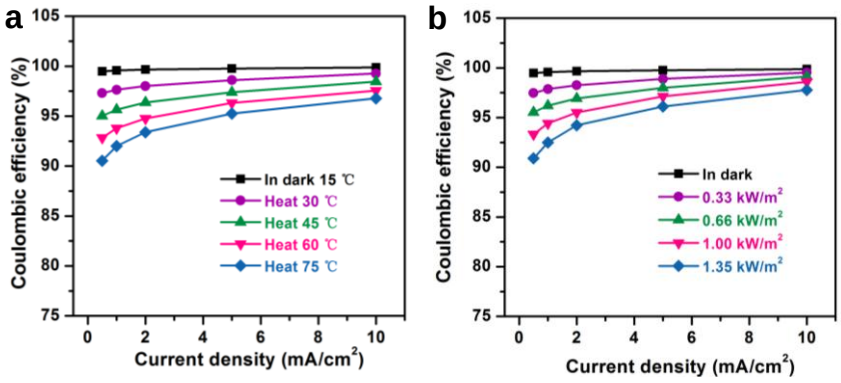


**Fig. S16** The coulombic efficiencies of the ST-MSC at different heating temperatures and under different solar light intensities.

**Table S4** Comparison of capacitance, energy density, and experiment conditions for the reported solar-heated supercapacitors

| Electrode materials | Electrolyte | Heating method | Potential window (V) | Specific capacitence ($F/cm^3$) | Energy density ($mWh/cm^3$) | Stability (capacitence retention) | Ref. |
|---|---|---|---|---|---|---|---|
| N-MCN @GH | PVA/$H_2SO_4$ | Solar heating in-situ from electrode material | 0-1.0 | 8.1 (R.T., 17 ℃)/4.05 (cooling to 5 ℃)/15.39 (cooling and under 3.6 solar irradiation) at 0.64 $mA/cm^2$ | 1.12 (R.T., 17 ℃)/0.56 (cooling to 5 ℃)/2.13 (cooling and under 3.6 solar irradiation) | 80 % (R.T., 17 ℃) after 10000 cycles | [11] |
| Graphene /PEDOT: PSS | PVA/$H_3PO_4$ | Solar heating in-situ from electrode material | 0-0.7 | 0.53 (R.T., 25 ℃)/0.82 (under 1 solar irradiation) at 3.3 $mA/cm^3$ | 0.036 (R.T., 25 ℃) / 0.056 (under 1 solar irradiation) | 99.76 % after 16000 cycles (R.T., 25 ℃)/72.04 % (under 1 solar irradiation) after 2000 cycles | [12] |
| PPy | PVA/$H_2SO_4$ | Solar heating ex-situ from additional graphene film | 0-0.6 | 12.08 (cooling to -50 ℃)/24.5 (cooling and under 1 solar irradiation) at 100 mV $s^{-1}$ | 0.96 (cooling to -50 ℃)/1.404 (cooling and under 1 solar irradiation) | 91.57% (cooling to -50 ℃)/98.41% (cooling and under 1 solar irradiation) after 5000 cycles | [13] |
| LIG/PPy | PVA/$H_2SO_4$ | Solar heating in-situ from electrode material | -0.6-0.7 | 19.1 (R.T., 15 ℃)/91.74 (R.T., under 1 solar irradiation)/4.25 (cooling to -30 ℃)/17.34 (cooling and under 1 solar irradiation) at 0.5 $mA/cm^2$ | 4.49 (R.T., 15 ℃)/ 21.53 (R.T., under 1 solar irradiation)/1.0 (cooling to -30 ℃)/4.08 (cooling and under 1 solar irradiation) | 96.3 % (R.T., 15 ℃)/85.8 % (R.T., under 1 solar irradiation)/82.4 % (cooling to -30 ℃)/95.2 % (cooling and under 1 solar irradiation) after 10000 cycles | This work |

**Note:** N-MCN@GH: N-doped mesoporous carbon nanosphere-intercalated 3D graphene hydrogel
PEDOT:PSS: Poly(3,4-ethylenedioxythiophene):Poly(sodium-p-styrenesulfonate)
1 solar irradiation intensity is 1.0 $kW/m^2$

**Fig. S17** Optical image of the low-temperature testing equipment (the ST-MSC placed and sealed in a homemade double-layer quartz container).

## Reference:


1 R. Q. Ye, D. K. James and J. M. Tour, *Adv. Mater.*, 2019, **31**, 1803621.

2 G. Chen, Y. Liu, F. Liu and X. Zhang, *Appl. Surf. Sci.*, 2014, **311**, 808

3 Z. Chen, W. Ren, L. Gao, B. Liu, S. Pei and H. M. Cheng, *Nat. Mater.*, 2011, **10**, 424.

4 C. Zhu, T. Y. J. Han, E. B. Duoss, A. M. Golobic, J. D. Kuntz, C. M. Spadaccini and M. A. Worsley, *Nat. Commun.*, 2015, **6**, 6962.

5 A. C. Ferrari, J. C. Meyer, V. Scardaci, C. Casiraghi, M. Lazzeri, F. Mauri, S. Piscanec, D. Jiang, K. S. Novoselov, S. Roth and A. K. Geim, *Phys. Rev. Lett*., 2006, **97**, 187401.

6 A. M. Dimiev, G. Ceriotti, N. Behabtu, D. Zakhidov, M. Pasquali, R. Saito and J. M. Tour, *ACS Nano*, 2013, **7**, 2773.

7 L. Li, J. B. Zhang, Z. W. Peng, Y. L. Li, C. T. Gao, Y. S. Ji, R. Q. Ye, N. D. Kim, Q. F. Zhong, Y. Yang, H. L. Fei, G. D. Ruan, and J. M. Tour, *Adv. Mater.*, 2016, **28**, 838-845.

8 H. Park, J. W. Kim, S. Y. Hong, G. Lee, D. S. Kim, J. h. Oh, S. W. Jin, Y. R. Jeong, S. Y. Oh, J. Y. Yun and J. S. Ha, *Adv. Funct. Mater.*, 2018, **28**, 1707013.

9 J. C. Chen, Y. M. Wang, J. Y. Cao, Y. Liu, Y. Zhou, J. H. Ouyang and D. C. Jia, *ACS Appl. Mater.*

*Inter.*, 2017, **9**, 19831-19842.

10 C. Yang, L. L. Zhang, N. T. Hu, Z. Yang, H. Wei and Y. F. Zhang, *J. Power Sources*, 2016, **302**, 39-45.

11 M. Y. Zhao, Y. L. Li, F. Lin, Y. S. Xu, L. L. Chen, W. C. Jiang, T. Jiang, S. G. Yang and Y. Wang, *J. Mater. Chem. A*, 2020, **8**, 1829-1836.

12 F. Yi, H. Y. Ren, K. R. Dai, X. F. Wang, Y. Z. Han, K. X. Wang, K. Li, B. L. Guan, J. Wang, M. Tang, J. Y. Shan, H. Yang, M. S. Zheng, Z. You, D. Wei and Z. F. Liu, *Energy Environ. Sci.*, 2018, **11**, 2016.

13 Y. L. Sun, P. J. Ma, L. Y. Liu, J. T. Chen, X. Zhang, J. W. Lang and X. B. Yan, *Sol. RRL*, 2018, **2**, 1800223.